# Mutations in *CLCN6* as a Novel Genetic Cause of Neuronal Ceroid Lipofuscinosis in Patients and a Murine Model

Hailan He, MD [1,2,3] Xiaoshuang Cao, MSc [1,2] Fang He, MD [1,2] Wen Zhang, MD [1,2] Xiaole Wang, MSc [1,2] Pan Peng, MSc [1,2] Changning Xie, MD [1,2] Fei Yin, MD [1,2] Dengfeng Li, PhD [4,5] Jiada Li, PhD [4,5] Minghui Wang, BSc [6] Malte Klüssendorf, PhD [7] Thomas J. Jentsch, MD PhD [8,9] Tobias Stauber, PhD [3,7†] and Jing Peng, MD [1,2†]

**Objective:** The aim of this study was to explore the pathogenesis of *CLCN6*-related disease and to assess whether its $Cl^-/H^+$-exchange activity is crucial for the biological role of ClC-6.
**Methods:** We performed whole-exome sequencing on a girl with development delay, intractable epilepsy, behavioral abnormities, retinal dysfunction, progressive brain atrophy, suggestive of neuronal ceroid lipofuscinoses (NCLs). We generated and analyzed the first knock-in mouse model of a patient variant (p.E200A) and compared it with a $Clcn6^{-/-}$ mouse model. Additional functional tests were performed with heterologous expression of mutant ClC-6.
**Results:** We identified a de novo heterozygous p.E200A variant in the proband. Expression of disease-causing ClC-$6^{E200A}$ or ClC-$6^{Y553C}$ mutants blocked autophagic flux and activated transcription factors EB (TFEB) and E3 (TFE3), leading to autophagic vesicle and cholesterol accumulation. Such alterations were absent with a transport-deficient ClC-$6^{E267A}$ mutant. $Clcn6^{E200A/+}$ mice developed severe neurodegeneration with typical features of NCLs. Mutant ClC-$6^{E200A}$, but not loss of ClC-6 in $Clcn6^{-/-}$ mice, increased lysosomal biogenesis by suppressing mTORC1-TFEB signaling, blocked autophagic flux through impairing lysosomal function, and increased apoptosis. Carbohydrate and lipid deposits accumulated in $Clcn6^{E200A/+}$ brain, while only lipid storage was found in $Clcn6^{-/-}$ brain. Lysosome dysfunction, autophagy defects, and gliosis were early pathogenic events preceding neuron loss.
**Interpretation:** *CLCN6* is a novel genetic cause of NCLs, highlighting the importance of considering *CLCN6* mutations in the diagnostic workup for molecularly undefined forms of NCLs. Uncoupling of $Cl^-$ transport from $H^+$ counter-transport in the E200A mutant has a dominant effect on the autophagic/lysosomal pathway.

**ANN NEUROL 2024;96:608–624**

The CLC family of chloride channels and transporters consists of 9 members, 4 (ClC-1, -2, -Ka, and -Kb) of which are plasma membrane chloride channels and 5 (ClC-3 to ClC-7) chloride/proton exchangers in endo-lysosomal membranes.[1] ClC-6, encoded by *CLCN6*, is one of the least-understood mammalian CLCs. *Clcn6*

View this article online at wileyonlinelibrary.com. DOI: 10.1002/ana.27002

Received Oct 16, 2023, and in revised form Apr 30, 2024. Accepted for publication May 8, 2024.

Address correspondence to Dr Tobias Stauber, Institute for Molecular Medicine, Medical School Hamburg, Am Kaiserkai 1, 20457 Hamburg, Germany. E-mail: tobias.stauber@medicalschool-hamburg.de, Dr Jing Peng, Department of Pediatrics, Xiangya Hospital, No.87, Xiangya Road, 410008, Changsha, China. E-mail: pengjing627@126.com

†These authors contributed equally to this work.

[Correction added on August 09, 2024, after initial online publication: In the article title, the text "in a Murine Model" has been added in this version.]

[Correction added on August 28, 2024, after initial online publication: In the article title, the text "Patients and" has been added in this version.]

From the [1]Department of Pediatrics, Xiangya Hospital, Central South University, Changsha, China; [2]Clinical Research Center for Children Neurodevelopmental Disabilities of Hunan Province, Changsha, China; [3]Institute of Chemistry and Biochemistry, Freie Universität Berlin, Berlin, Germany; [4]Center for Medical Genetics, School of Life Sciences, Central South University, Changsha, China; [5]Hunan Key Laboratory of Animal Models for Human Diseases, Central South University, Changsha, China; [6]The First People's Hospital of Changde, Changde, China; [7]Institute for Molecular Medicine, MSH Medical School Hamburg, Hamburg, Germany; [8]Leibniz-Forschungsinstitut für Molekulare Pharmakologie (FMP) and Max-Delbrück-Centrum für Molekulare Medizin (MDC), Berlin, Germany; and [9]NeuroCure Cluster of Excellence, Charité Universitätsmedizin Berlin, Berlin, Germany

Additional supporting information can be found in the online version of this article.

 

mRNA is expressed ubiquitously,[2] whereas the ClC-6 protein is predominantly found in the nervous system where it resides on late endosomes.[3] *Clcn6*$^{-/-}$ mice are viable, fertile, and have only mild behavioral abnormalities without neuron loss.[3] However, they display a mild accumulation of lysosomal storage material in axon initial segments.[3] The mechanism underlying this pathology and the precise physiological role of ClC-6 remains largely enigmatic. Unexpectedly, human genetics revealed an important, but poorly understood, role of ClC-6 in the brain. So far, 3 heterozygous disease-associated *CLCN6* variants (p.E200A, p.Y553C, p.T520A) have been identified in patients with epileptic encephalopathy and early onset neurodegeneration, respectively.[4–8] The severe neurological symptoms in individuals with heterozygous *CLCN6* variants contrasts strikingly with the mild phenotype in *Clcn6*$^{-/-}$ mice and apparently unaffected heterozygous *Clcn6*$^{+/-}$ mice.[3,4,6] This suggests that in patients, monoallelic variants of *CLCN6* induce neurological defects through a gain, rather than loss-of-function. Indeed, the ClC-6$^{Y553C}$ and very recently the ClC-6$^{T520A}$ variants were shown to mediate current with larger amplitudes, likely because the voltage-dependence of its activation is shifted to less cytosolic-positive voltages.[6,8,9]

ClC-6 is an electrogenic $2Cl^-/H^+$ exchanger which mediates the exchange of $Cl^-$ against $H^+$.[10] The CLC family members share a critical glutamate residue in the ion permeation pathway that is involved in gating of CLC channels and in coupling $Cl^-$ to $H^+$ fluxes of CLC exchangers, respectively.[1] Like for other vesicular CLC exchangers, the mutation of the gating glutamate abolished ClC-6-mediated $H^+$ transport, and converted the strongly voltage-dependent $Cl^-/H^+$-exchange of ClC-6 into a pure anion conductance.[10] Recently, we reported a de novo heterozygous *CLCN6* p.E200A variant of the critical gating glutamate in a patient with early-onset epilepsy, visual impairment, autism, and cognitive deficit.[4] Equivalent uncoupling mutations in other CLC exchangers lead to pathology in mice models and human patients.[11–14]

Here, we analyzed clinical and genetic characteristics of a 10-year-old girl with a de novo heterozygous p.E200A variant and generated the first knock-in mouse model harboring the uncoupling p.E200A mutation, to investigate the pathogenesis of *CLCN6*-related disease and to assess the relevance of $Cl^-/H^+$-exchange activity for the physiological role of ClC-6. The patient showed intractable epilepsy, behavioral abnormities, retinal dysfunction, progressive brain atrophy, suggestive of neuronal ceroid lipofuscinoses (NCLs). Studies in cellular model systems showed that overexpression of disease-causing ClC-6 mutants impaired the lysosomal degradation of autophagic material, and influenced cholesterol metabolism. The mouse model harboring the heterozygous p.E200A variant phenocopies the *CLCN6* p.E200A patients and exhibits characteristic features of NCLs. Our molecular analysis shows that disease-causing *CLCN6* mutations result in defective mTORC1 signaling, specifically in the transcription factor EB (TFEB)/transcription factor E3 (TFE3) axis regulating autophagy and lysosome function.

## Methods

### Study Patient

The proband was referred to the Department of Pediatrics, Xiangya Hospital, Central South University, China. The study involving human subjects received approval from the Ethics Committee at Xiangya Hospital of Central South University (approval ID: #201703240) and was conducted in accordance with the ethical principles of the Declaration of Helsinki. Written informed consent was obtained from the proband's parents.

### Whole Exome Sequencing (WES)

Peripheral blood was collected from the patient and her parents. WES sequencing was performed as previously described.[15]

### Animals

All animal experiments were performed according to the guidelines of Laboratory Animal Manual of the National Institute of Health Guide to the Care and Use of Animals, which were approved by the Institutional Animal Care and Use Committee of the Xiangya Hospital of Central South University (approval ID: #201703241). Mice were housed in the Central South University genetic animal facility or Delbrück-Centrum für Molekulare Medizin animal facility (approved by and in compliance with local authorities, LAGeSo Berlin, Germany). *Clcn6*$^{E200A/+}$ knock-in and *Clcn6*-knockout mice were generated by the Nanjing Biomedical Research Institute using CRISPR/Cas9 genome-editing technology. Details are described in the supporting information.

### Histological and Histochemical Analyses

Histological and histochemical analyses are described in detail in the supporting information.

### Statistical Analysis

Statistical analyses were performed using GraphPad Prism version 6. Statistical differences were analyzed using 1-way analysis of variance (ANOVA) or nonparametric, followed by Tukey's multiple comparisons test. Data are represented as mean ± SEM. *p*-Values are depicted as: $*p < 0.05$; $**p < 0.01$; $***p < 0.001$.

## Results

### Clinical Findings

The proband is a 10-year-old girl with severe developmental delay, intractable epilepsy, behavioral abnormities, and microcephaly. A delay in P100 wave latency was observed in the visual evoked potential (Fig 1A). Brain MRI showed progressive cerebellar and cerebral atrophy co-occurring with enlargement of the lateral ventricles (Fig 1B). Electroencephalography (EEG) recordings revealed interictal bilateral sharp waves, spike waves, sharp and slow wave complexes, spike and slow wave complexes in bilateral frontal pole, frontal, anterior temporal region at 10 years (Fig 1C). WES and Sanger sequencing revealed that she has a heterozygous de novo *CLCN6* c.599A > C, p.E200A variant (Fig 1D). With the proband, the total number of patients with *CLCN6* disease-causing variants known to date is 6 (2 with the E200A variant, 3 with the p.Y553C variant, 1 with the p.T520A variant).[4,6,8] They share some clinical features: global developmental delay, developmental regression, visual impairments, and brain imaging abnormalities,[4,6,8] suggestive of NCLs. Further clinical details are described in the supporting information and Table S1.

### Alterations of the Autophagic-Lysosomal Pathway (ALP) and TFEB/TFE3 Signaling and Accumulation of Free Cholesterol with Disease-Causing ClC-6 Mutants

To investigate the effects of *CLCN6* mutations in the ALP, we expressed the p.E200A and p.Y553C patient mutants and the p.E267A mutant, which almost completely abolishes both $Cl^-$ and $H^+$-transport by ClC-6,[9,10] in HeLa cells. We found that the microtubule-associated protein 1 light chain 3-II (LC3-II)/LC3-I ratio as well as protein levels of sequestosome 1 (SQSTM1/p62) were significantly increased upon expression of the p.E200A and p.Y553C mutants compared to wild-type (WT) ClC-6-transfected cells, whereas no such effect was found with the p.E267A mutant (Figs 2A and S1). These findings suggest an impairment of the ALP by the 2 disease-causing ClC-6 mutants, but not with the nearly transport-deficient p.E267A mutant.

Since TFEB and TFE3 are master regulators of ALP,[16–18] we examined the nuclear translocation of enhanced green fluorescent protein (eGFP)-tagged TFEB and TFE3 in HeLa cells together with either WT or mutant ClC-6. Coexpression with the mutants p.E200A or p.Y553C, but not p.E267A, resulted in a drastic increase of nuclear eGFP-TFEB and eGFP-TFE3 (Fig 2B,C), compared with WT ClC-6 coexpression. These observations indicate an activation of TFEB and TFE3 signaling by the presence of the disease-causing ClC-6 mutants.

In order to test whether further functions of lysosomes are impaired, we assessed free cholesterol levels by Filipin staining, and found more Filipin staining in cells expressing ClC-$6^{E200A}$ or ClC-$6^{Y553C}$ mutants than in cells expressing WT ClC-6 or ClC-$6^{E267A}$ mutant (Figs 2D and S2). These results suggest an accumulation of free cholesterol upon expression of disease-causing mutant ClC-6.

### Neurological Phenotypes of Clcn6$^{E200A/+}$ Mice

*Clcn6*$^{E200A/+}$ and *Clcn6*$^{-/-}$ mice were generated using CRISPR/Cas9 technology (Fig S3). As we failed to mate heterozygous *Clcn6*$^{E200A/+}$ with WT mice, sperm of male *Clcn6*$^{E200A/+}$ mice were used for in vitro fertilization. *Clcn6*$^{E200A/+}$ and *Clcn6*$^{-/-}$ mice were born with Mendelian ratio. However, the survival rate of *Clcn6*$^{E200A/+}$ mice dropped markedly by 4 months. All *Clcn6*$^{E200A/+}$ mice died within 7 months (Fig 3A), accompanied by a weight loss after 24 weeks (Fig 3B). Furthermore, *Clcn6*$^{E200A/+}$ mice manifested neurological deterioration attested by abnormal limb-clasping reflexes by 8 weeks (Fig 3C). Disease symptoms progressed rapidly with the onset of a tremor at 3 months that became progressively more severe and was accompanied by locomotor difficulties including hunched gait and ataxia (Movies S1 and S2). In contrast, as reported for a previously generated mouse line,[3] homozygous *Clcn6*$^{-/-}$ and heterozygous *Clcn6*$^{+/-}$ mice were indistinguishable in this respect from their WT littermates and had a normal lifespan.

In p.E200A patients, brain MRI shows brain atrophy (this study and ref[4]). Similarly, high-resolution MRI revealed a significant decrease in brain volume and enlarged ventricles of 5-month-old *Clcn6*$^{E200A/+}$ mice (Fig 3D). Remarkably, although our tests revealed no neurological phenotypes in *Clcn6*$^{-/-}$ mice, similar dilation of lateral ventricles was observed (Fig 3D).

Like for the p.E200A patients (this study and ref[4]), seizures were observed in 4- to 5-month-old *Clcn6*$^{E200A/+}$ mice, but not in *Clcn6*$^{-/-}$ mice (Movies S3–S6). Importantly, video EEG recordings showed massive spike–wave and rhythmic spikes discharges in *Clcn6*$^{E200A/+}$ mice, whereas only few low-amplitude spike waves were observed in age-matched *Clcn6*$^{-/-}$ mice (Fig 3E). We did not observe a direct link between the seizures and the death of the mice as recently shown for mice with a pathogenic *Cln2* variant.[19]

To test for retinal dysfunction, as found for the p.E200A patients (this study and ref[4]) we performed electroretinographic (ERG) analyses. The b-wave response

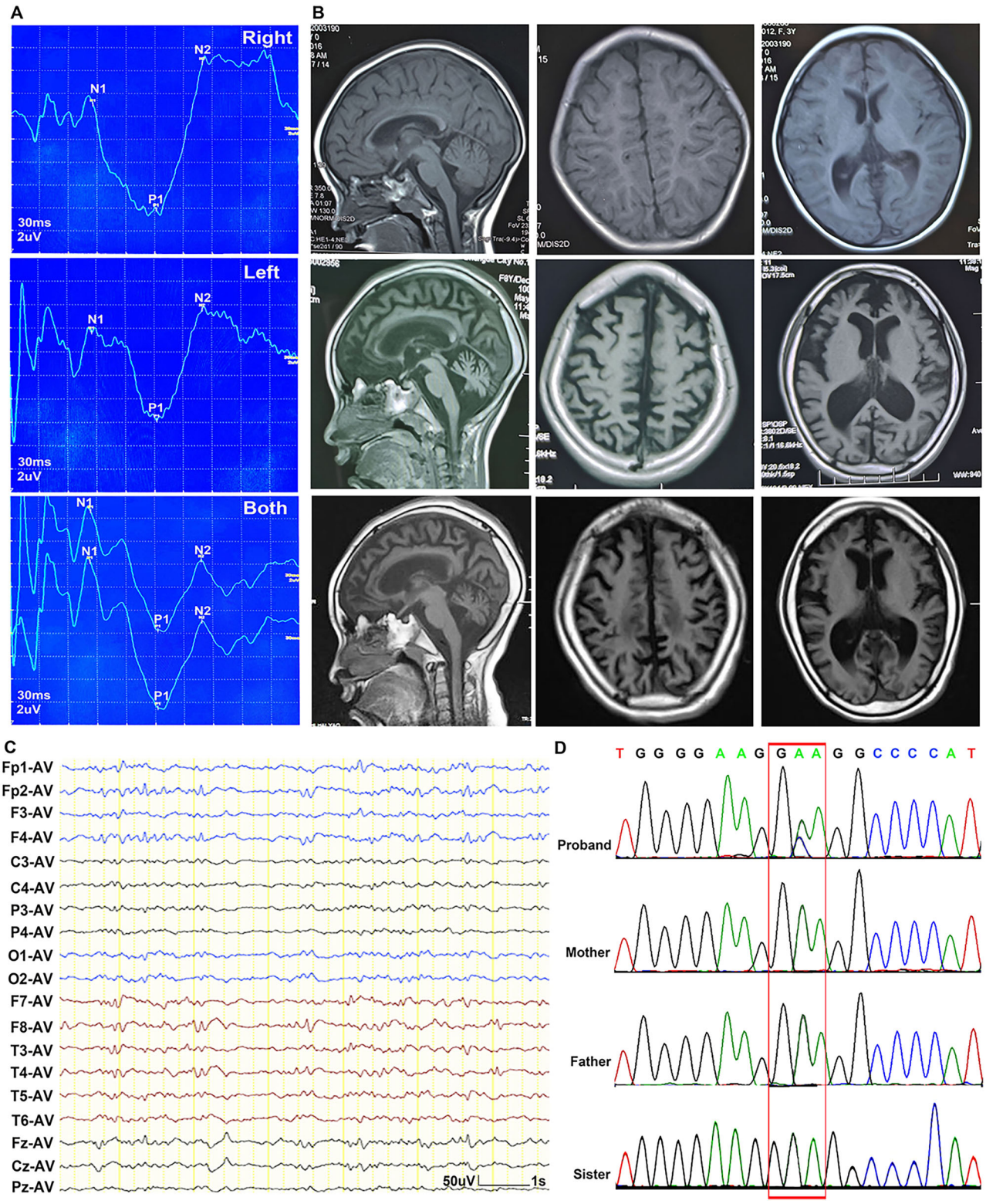


**FIGURE 1:** Clinical data of the patient. (A) Visual evoked potential test at 10 years showed a delay in P100 wave latency. (B) Brain MRI (T1-weighted, sagittal, and coronal planes) of the patient at the age of 4 years (*top row*), the age of 8 years (*middle row*), and the age of 10 years (*bottom row*) showing progressive cerebellar and cerebral atrophy with a secondary hydrocephalus. (C) Video EEG at 10 years of age showing interictal bilateral sharp waves, spike waves, sharp and slow wave complexes, spike and slow wave complexes were evident in bilateral frontal pole, frontal, anterior temporal region. (D) Sanger sequence chromatograms showing a de novo heterozygous constitutive c.599A > C in *CLCN6*. [Color figure can be viewed at www.annalsofneurology.org]

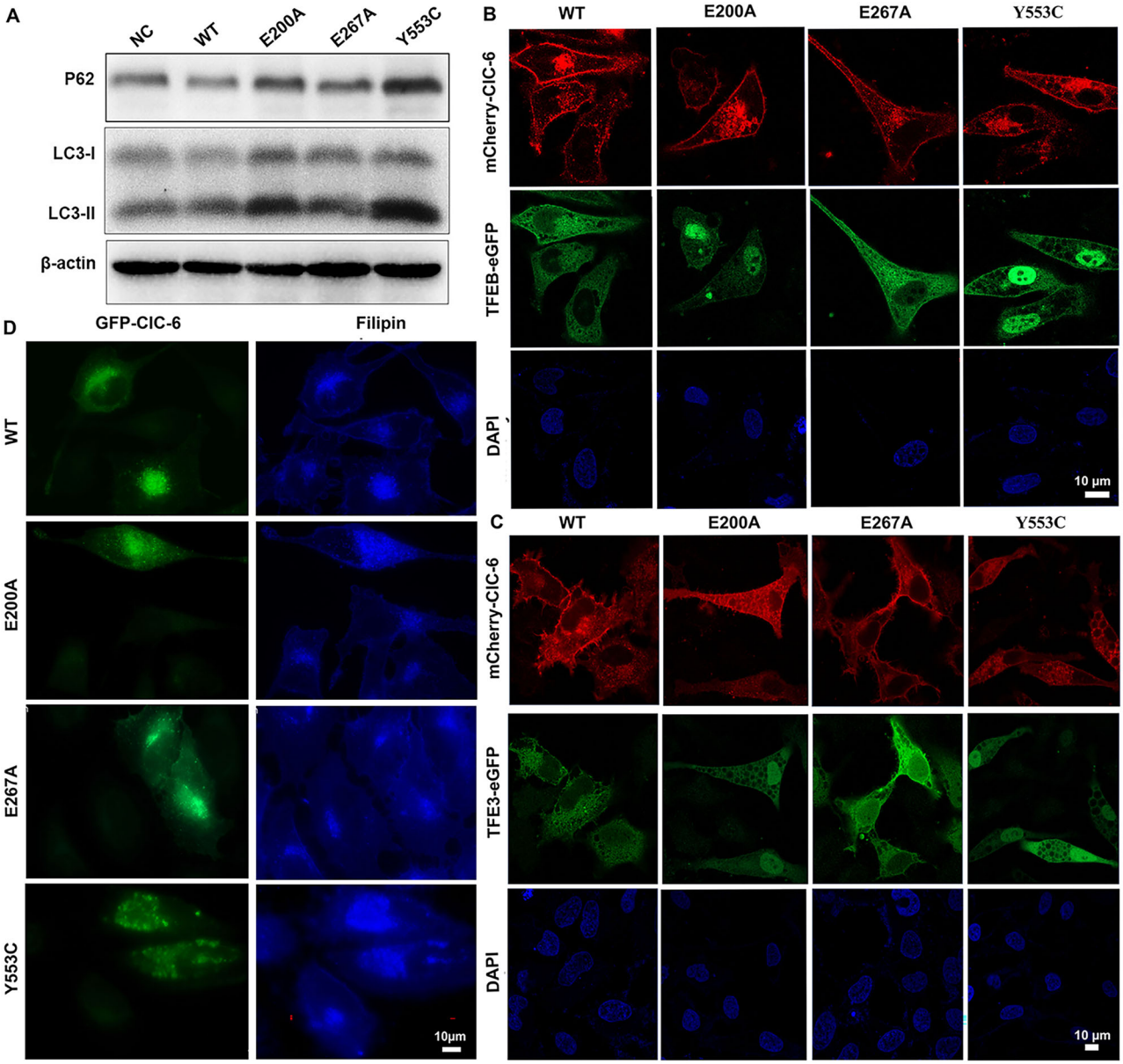


**FIGURE 2: Effect of *CLCN6* variants on TFEB/TFE3-autophagy-lysosome pathway and free cholesterol. (A) The LC3-II/LC3-I ratio and protein levels of SQSTM1/p62 were significantly increased upon expression of the p.E200A and p.Y553C mutants compared to WT ClC-6-transfected cells, whereas no such effect was found in cells expressing the p.E267A mutant. For quantification, see Figure S1. (B, C) Coexpression of the mutants p.E200A or p.Y553C, but not p.E267A, resulted in a drastic increase of nuclear eGFP-TFEB (B) and eGFP-TFE3 (C) compared with WT ClC-6 coexpression. (D) Cells expressing ClC-6$^{E200A}$ or ClC-6$^{Y553C}$ mutants showed more filipin staining than cells expressing WT ClC-6 or ClC-6$^{E267A}$ mutant. For quantification, see Figure S2. Scale bar, 10 μm. [Color figure can be viewed at www.annalsofneurology.org]**

amplitudes were dramatically reduced in all dark and light adapted tests, as well as both scotopic and photopic a-wave response amplitudes at any stimulus intensity level, with the only exception at a flash strength of 3 cd.s/m$^2$ in 4–6 months old *Clcn6*$^{E200A/+}$ mice (Fig 3F). In *Clcn6*$^{-/-}$ mice, the scotopic b-wave amplitudes also decreased significantly, but more mildly at all level stimulus intensities, and the photopic b-wave responses were much weaker compared to WT controls at 10 and 30 cd.s/m$^2$ (Fig 3F). These data indicate retinal dysfunction in both *Clcn6*$^{E200A/+}$ and *Clcn6*$^{-/-}$ mice. However, hematoxylin and eosin (H&E) staining revealed no retina degeneration in 5-month-old *Clcn6*$^{E200A/+}$ or, as previously shown,[3] *Clcn6*$^{-/-}$ mice (Fig S4).

### *Behavioral Abnormalities of* Clcn6$^{E200A/+}$ *Mice*

Next, we performed a battery of behavioral assays with 1, 3, and 5 months old WT, *Clcn6*$^{E200A/+}$ and *Clcn6*$^{-/-}$

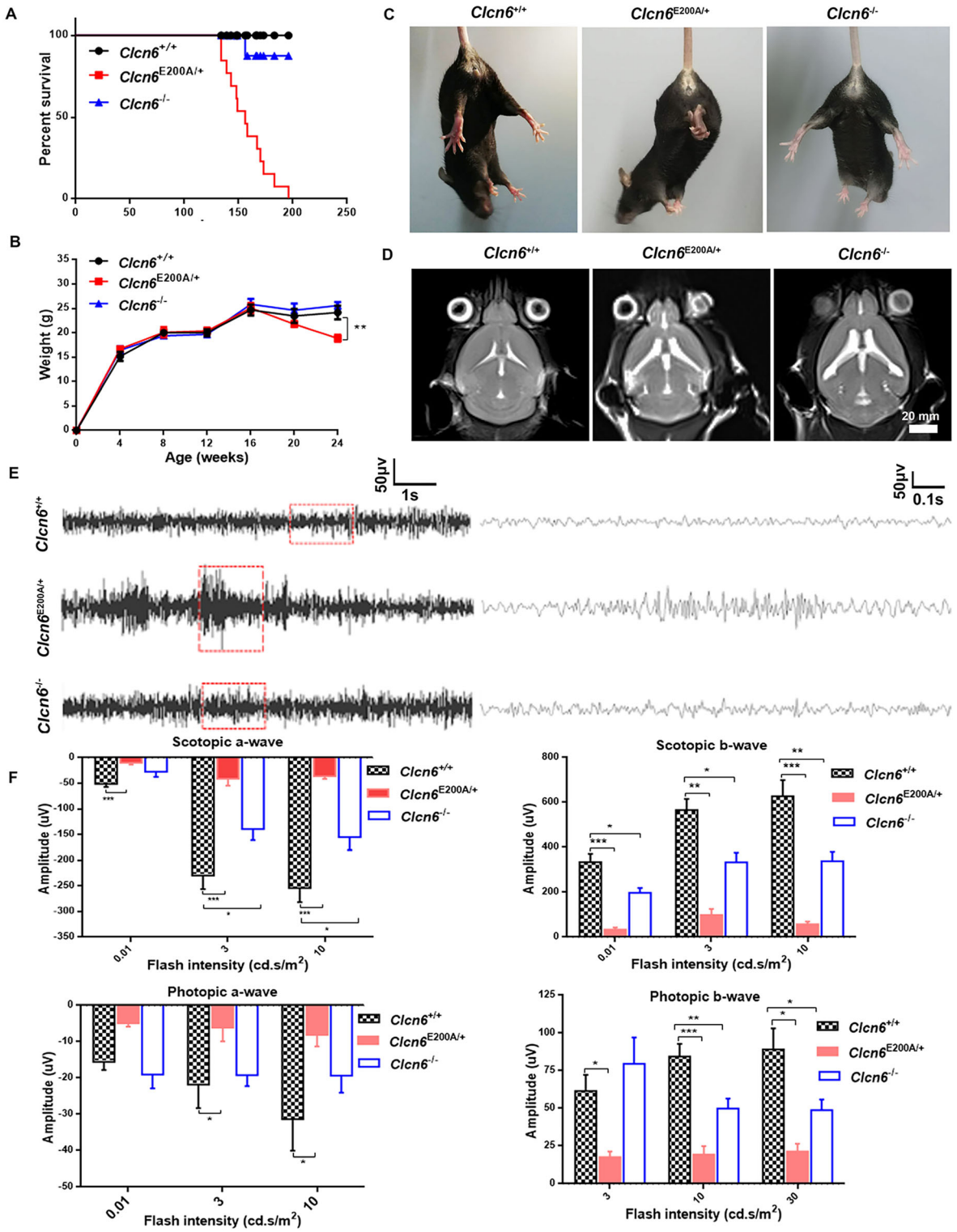


FIGURE 3: Phenotypes of *Clcn6*$^{E200A/+}$ and *Clcn6*$^{-/-}$ mice. (A) Survival analysis indicated reduced lifespan of *Clcn6*$^{E200A/+}$ mice. n ≥ 15 per genotype. (B) Body mass was reduced in *Clcn6*$^{E200A/+}$ mice at 24 weeks (near the terminal stage), but not in *Clcn6*$^{-/-}$ mice. n ≥ 8 per genotype. (C) *Clcn6*$^{E200A/+}$ mice, but not *Clcn6*$^{-/-}$ mice manifested clasping behavior. n ≥ 12 per genotype. (D) The 5-month-old *Clcn6*$^{E200A/+}$ mice displayed a significant decrease of brain volume, and enlarged ventricles. Similar dilation of lateral ventricles, but no changes in brain volume was observed in 5-month-old *Clcn6*$^{-/-}$ mice as assessed by brain MRI. Scale bar: 20 mm. (E) EEG recordings showed massive spike–wave and rhythmic spike discharges in 4-to-5-month-old *Clcn6*$^{E200A/+}$ mice, whereas only a few low-amplitude spike waves were seen in age-matched *Clcn6*$^{-/-}$ mice. (F) ERG recordings showed both a- and b-waves were markedly reduced in *Clcn6*$^{E200A/+}$ mice. [Color figure can be viewed at www.annalsofneurology.org]

mice. Balance beam and rotarod tests revealed impaired motor coordination at all ages in *Clcn6*$^{E200A/+}$ mice, characterized by a longer latency to cross the beam and a shorter latency to fall off the rod starting at 1 month, and higher number of foot slips starting at 3 months (Figs S5A and S5B). Likewise, we also observed an abnormal gait with markedly wide-based stance, small stride, and separated hindlimb prints in *Clcn6*$^{E200A/+}$ mice (Fig S5C). At 5 months, *Clcn6*$^{E200A/+}$ mice scored drastically lower than WT controls in both coat-hanger and hanging wire tests (Figs S5D and S5E), indicating decreased muscle strength. In the open field test, *Clcn6*$^{E200A/+}$ mice showed a longer total track length at 3 months, whereas they traveled significantly less spontaneously at 5 months compared to age-matched WT controls (Fig S5F), indicating hyperactivity in the early stage and a decreased exploratory activity at the end stage. Dwell time in center field was strongly decreased at 3 months (Fig S5F), consistent with anxiety-like phenotypes. In contrast, *Clcn6*$^{-/-}$ mice behaved similarly to WT controls in all the tests except for the open field assay, where they exhibited anxiety-like phenotypes at 5 months (Fig S5A–F).

### *Progressive Neurodegeneration and Early Glial Responses in* Clcn6$^{E200A/+}$ *Brain*

As MRI showed brain atrophy in the *Clcn6*$^{E200A/+}$ mice, we measured brain weights among the 3 genotypes. *Clcn6*$^{E200A/+}$ mice possessed significantly smaller brains with reduced weight compared to WT littermates or *Clcn6*$^{-/-}$ counterparts at 4 months, but not at P30 (Figs 4A and S6). As there was no significant difference in body weight between the genotypes at these ages, these results point toward a brain degeneration in *Clcn6*$^{E200A/+}$ mice. In addition, cortex thickness measurement revealed widespread atrophy of the cortex in 5-month-old *Clcn6*$^{E200A/+}$ mice that was not evident in age-matched *Clcn6*$^{-/-}$ mice (Fig. S7). Therefore, we examined the onset and progression of neuropathological changes systematically in *Clcn6*$^{E200A/+}$ and *Clcn6*$^{-/-}$ mice at postnatal days P30, P60, P90, P120, and P150. We found that neuron loss in *Clcn6*$^{E200A/+}$ mice became firstly apparent in the cornu ammonis (CA) 3 region of the hippocampus at P60 (Fig 4B). Loss of Purkinje cells was seen as early as P90 (Fig 4C), in agreement with the development of tremor and ataxia around this time. Specifically, the loss of Purkinje cells started preferentially, and was particularly pronounced in lobule I and lobule II of the cerebellum. At the end stage, immunohistochemical staining for the Purkinje cell marker calbindin revealed almost complete loss of Purkinje cells, except for lobules IX and X, in *Clcn6*$^{E200A/+}$ mice (Fig S8). On the other hand, histological staining of *Clcn6*$^{-/-}$ brain sections revealed no morphological abnormalities up to 20 months (Figs 4C and S9). Assessment of survival of interneurons in the cortex and hippocampus of *Clcn6*$^{E200A/+}$ mice revealed loss of somatostatin-positive (SST+) neurons, but not of parvalbumin-positive (PV+) or calretinin-positive (CR+) neurons (Figs S10–S12). Luxol-fast blue staining revealed a clear disruption of myelin in the brain of 5-month-old *Clcn6*$^{E200A/+}$ mice and mildly disturbed myelination in *Clcn6*$^{-/-}$ mice (Fig 4D). Together, these data demonstrated brain atrophy and degeneration in *Clcn6*$^{E200A/+}$ mice.

Neurodegeneration was paralleled by an activation of astrocytes and microglia, as revealed by astrocyte marker glial fibrillary acidic protein (GFAP) and microglia marker ionized calcium binding adaptor molecule 1 (IBA-1) staining of the brain from 4-to-5-month-old *Clcn6*$^{E200A/+}$ mice (Figs 4E, S13 and S14) and immunoblotting (Fig S15). To test whether glial activation precedes or follows neuron loss, we examined astrocytes and microglia in presymptomatic P30 *Clcn6*$^{E200A/+}$ mice, when degeneration is observed in neither these, nor in *Clcn6*$^{-/-}$ mice (Fig 4F). In P30 *Clcn6*$^{E200A/+}$ mice, GFAP and IBA-1 immunoreactivity was prominent and morphologically similar to that observed at 4 months, but was less markedly different from WT controls (Figs 4F and S16–S19). On the other hand, *Clcn6*$^{-/-}$ brain sections revealed no astrogliosis or microgliosis at any age tested (Figs 4E,F and S13–17). Taken together, *Clcn6*$^{E200A/+}$ mice exhibit early and progressive astrocytic and microglial reactive changes, events occurring before obvious neuron loss.

### *Accumulation of Autofluorescent Lysosomal Storage Material in* Clcn6$^{E200A/+}$ *Neurons*

We observed widespread intracellular accumulation of autofluorescent storage material in many brain regions of *Clcn6*$^{E200A/+}$ mice at 5 months (Fig 5A). Interestingly, while storage material was present predominantly in the proximal axon in *Clcn6*$^{-/-}$ mice as shown previously,[3] it was scattered in punctate structures over the neuronal soma and axon of *Clcn6*$^{E200A/+}$ mice.

To examine the morphology of the deposits in more detail, we performed electron microscopy of cortex, hippocampus, and cerebellum. This revealed abnormal electron-dense lysosomal storage material in the somata of *Clcn6*$^{E200A/+}$ neurons and in the proximal axon of *Clcn6*$^{-/-}$ neurons at 5 months (Fig 5B). Higher magnification of deposits showed an accumulation of lysosomes, autophagosomes, numerous intracellular inclusion bodies with double membranes or multilamellated electron-dense material, damaged organelles, lipid droplets,

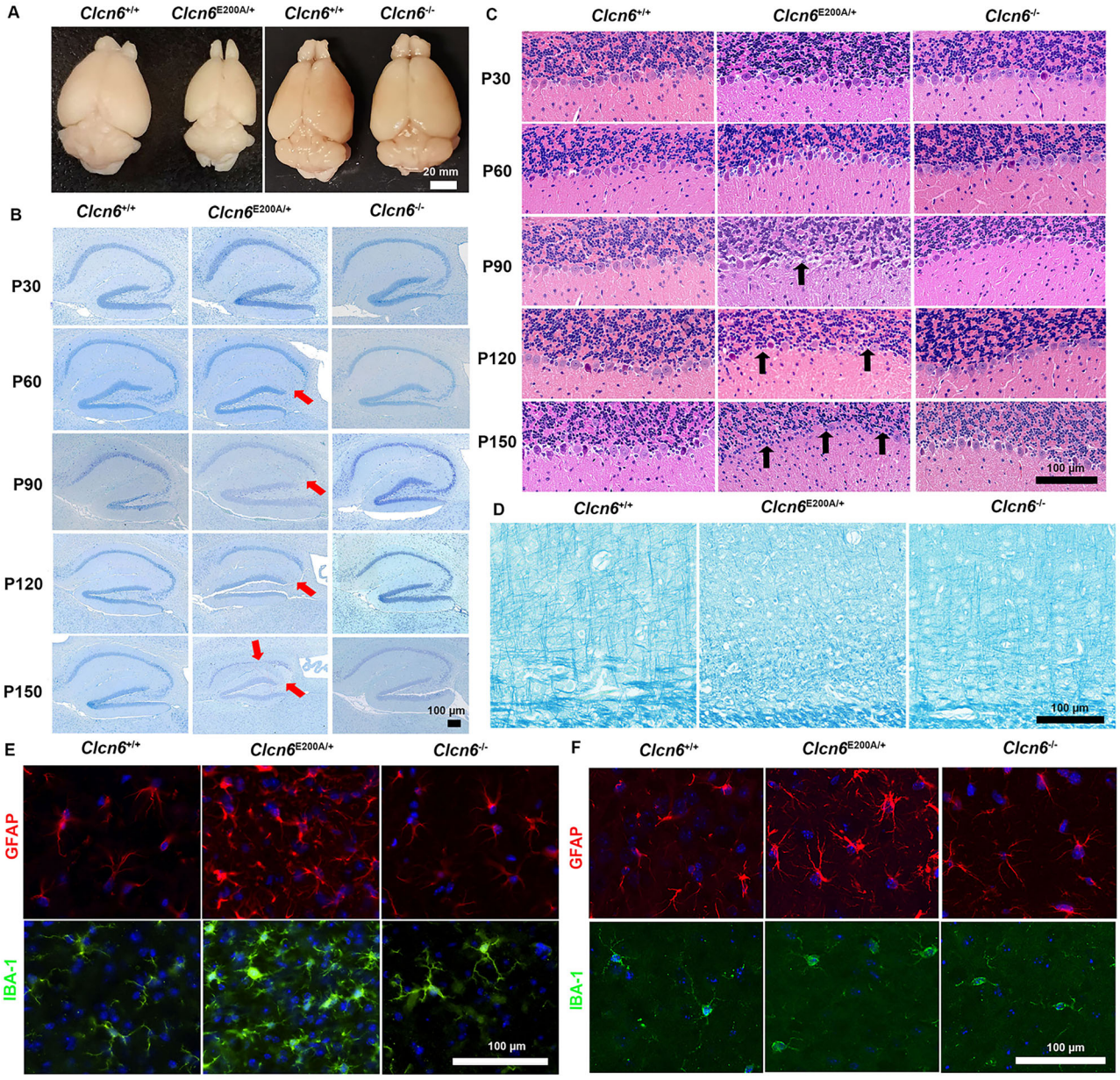


**FIGURE 4: Neuropathology in brains from *Clcn6*$^{E200A/+}$ and *Clcn6*$^{-/-}$ mice. (A) Morphology of the brain from representative heterozygous *Clcn6*$^{E200A/+}$, *Clcn6*$^{-/-}$ mice, and their WT littermate. Note that the decreased brain sizes in *Clcn6*$^{E200A/+}$ mice are visually appreciable compared to those of the *Clcn6*$^{-/-}$ and WT mice. (B) Nissl-stained sagittal sections of WT, *Clcn6*$^{E200A/+}$, and *Clcn6*$^{-/-}$ hippocampi from P30 to P150 indicates onset of neuron loss of the hippocampal CA3 region in *Clcn6*$^{E200A/+}$ mice at P60 (arrows). (C) Representative H&E-stained WT, *Clcn6*$^{E200A/+}$ and *Clcn6*$^{-/-}$ cerebellums from P30 to P150 shows progressive loss of Purkinje cells (arrows) in the cerebellum of *Clcn6*$^{E200A/+}$ mice compared to WT mice starting at P90. (D) Luxol fast blue staining of paraffin-embedded brain sections (representative images of the secondary motor cortex shown) reveals disturbed myelination in both *Clcn6*$^{E200A/+}$ and *Clcn6*$^{-/-}$ mice. (E-F) Immunofluorescence staining for the astrocyte marker GFAP (red) and the microglial marker IBA-1 (green) reveal astrogliosis and microgliosis in the brain (representative confocal images of the secondary motor cortex) of *Clcn6*$^{E200A/+}$ mice at both 4 months (E) and P30 (F) of age compared to age matched WT mice. (B-F) Astrogliosis and microgliosis are not observed in *Clcn6*$^{-/-}$ mice. Scale bars: 20 mm (A), 100 µm (B-F).**

amorphous or granular lipofuscin deposits in the neurons of *Clcn6*$^{E200A/+}$ mice (Fig 5C–L), whereas *Clcn6*$^{-/-}$ neurons only showed lipid droplets associated with electron-dense amorphous or granular lipofuscin deposits in the proximal axons (Fig 5M,N). The aberrant accumulation of organelles and storage material in neurons of *Clcn6*$^{E200A/+}$ mice is a characteristic feature of NCLs. In addition, autophagosomes and lysosomes were significantly larger in neurons of *Clcn6*$^{E200A/+}$ compared to WT mice (Fig 5), which suggest that autophagy and lysosomal degradation are disturbed in *Clcn6*$^{E200A/+}$ mice.

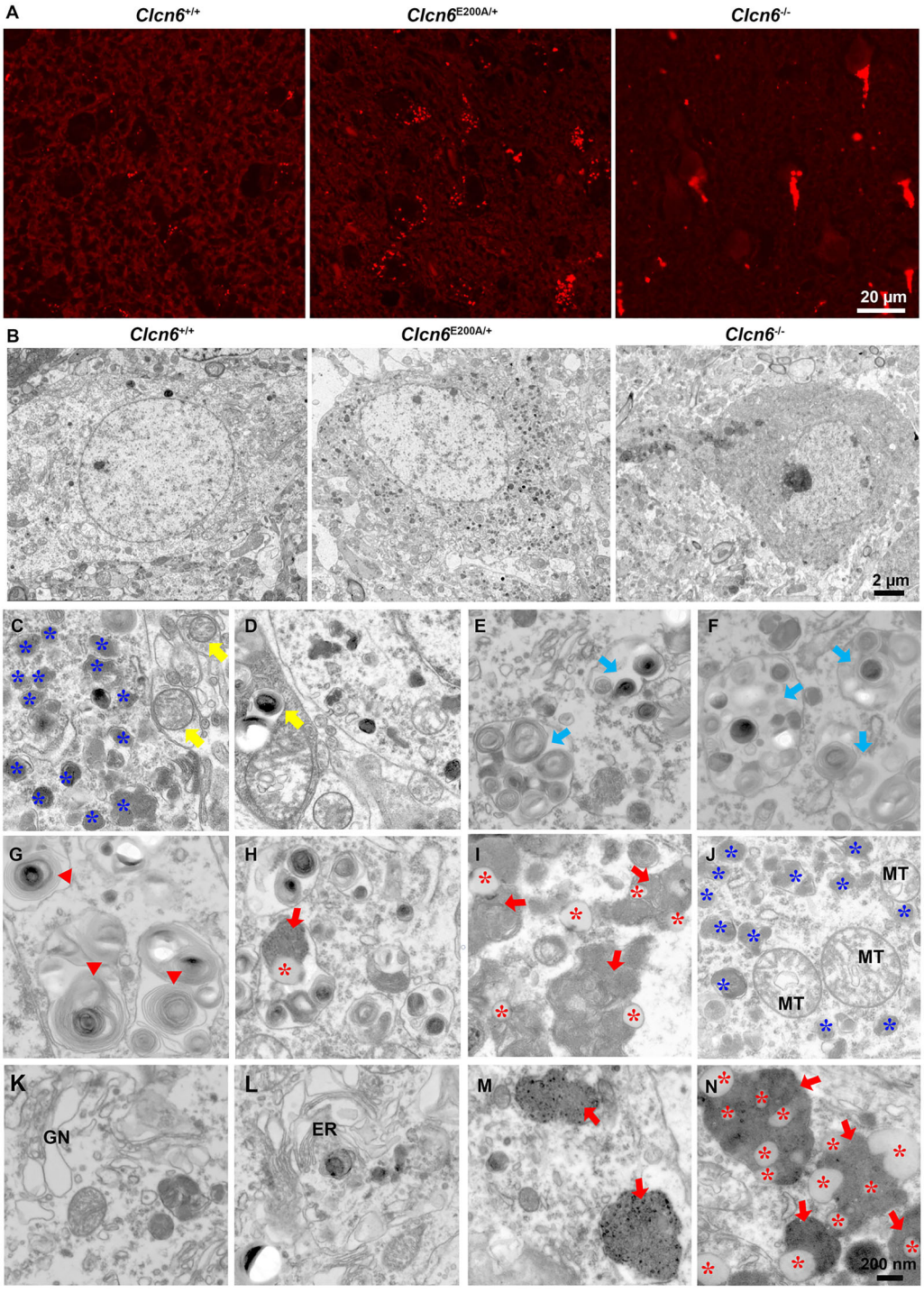


FIGURE 5: Accumulation of neuronal autofluorescent lysosomal storage material in *Clcn6*$^{E200A/+}$ mice. (A) Representative images of the frontal cortex in unstained brain sections visualized at 543 ± 11 nm excitation and 593 ± 20 nm detection show the abundant intracellular accumulation of autofluorescent storage material in neuronal soma and axon of 5-month-old *Clcn6*$^{E200A/+}$ mice compared with age-matched WT controls. While autofluorescence is visible in the proximal axon of 5-month-old *Clcn6*$^{-/-}$ mice. (B) Electron micrographs showed massive electron-dense lysosomal storage material in the perikaryal of *Clcn6*$^{E200A/+}$ neurons (representative images of the frontal cortex), which is less abundant in the neurons of *Clcn6*$^{-/-}$ mice and only locates in the proximal axon of *Clcn6*$^{-/-}$ neurons. (C-L) Higher magnification shows an accumulation of lysosomes (*blue asterisks*), double membraned autophagosomes (*yellow arrows*), numerous intracellular inclusion bodies (*blue arrows*) with double membranes or multilamellated electron-dense material (red arrowhead), damaged organelles, lipid droplets (*red asterisks*), amorphous or granular lipofuscin deposits (*red arrows*) in neurons of *Clcn6*$^{E200A/+}$ mice. (M,N) Higher magnification demonstrates only lipid droplets associated with electron-dense amorphous or granular lipofuscin deposits in neurons of *Clcn6*$^{-/-}$ mice. No lysosomes, autophagosomes, intracellular inclusion bodies, or damaged organelles were observed. MT = mitochondrium, ER = endoplasmic reticulum, GN = Golgi. Scale bars: 20 µm (A), 2 µm (B), 200 nm (C-N).

### *Metabolic Disorder in* Clcn6$^{E200A/+}$ *Brain*

To assess brain carbohydrate accumulation in *Clcn6*$^{E200A/+}$ and *Clcn6*$^{-/-}$ mice, we performed periodic acid Schiff (PAS) staining in 5-month-old WT, *Clcn6*$^{E200A/+}$ and *Clcn6*$^{-/-}$ mice. We observed PAS-positive granular deposits not only in the perikaryon of neurons, but also in the intercellular space of cortex, hippocampus, and cerebellum of *Clcn6*$^{E200A/+}$ mice (Fig 6A). By contrast, in *Clcn6*$^{-/-}$ mice, no positive labeling with PAS staining was detectable (Fig 6A). Next, we measured lipids in the brain of WT,

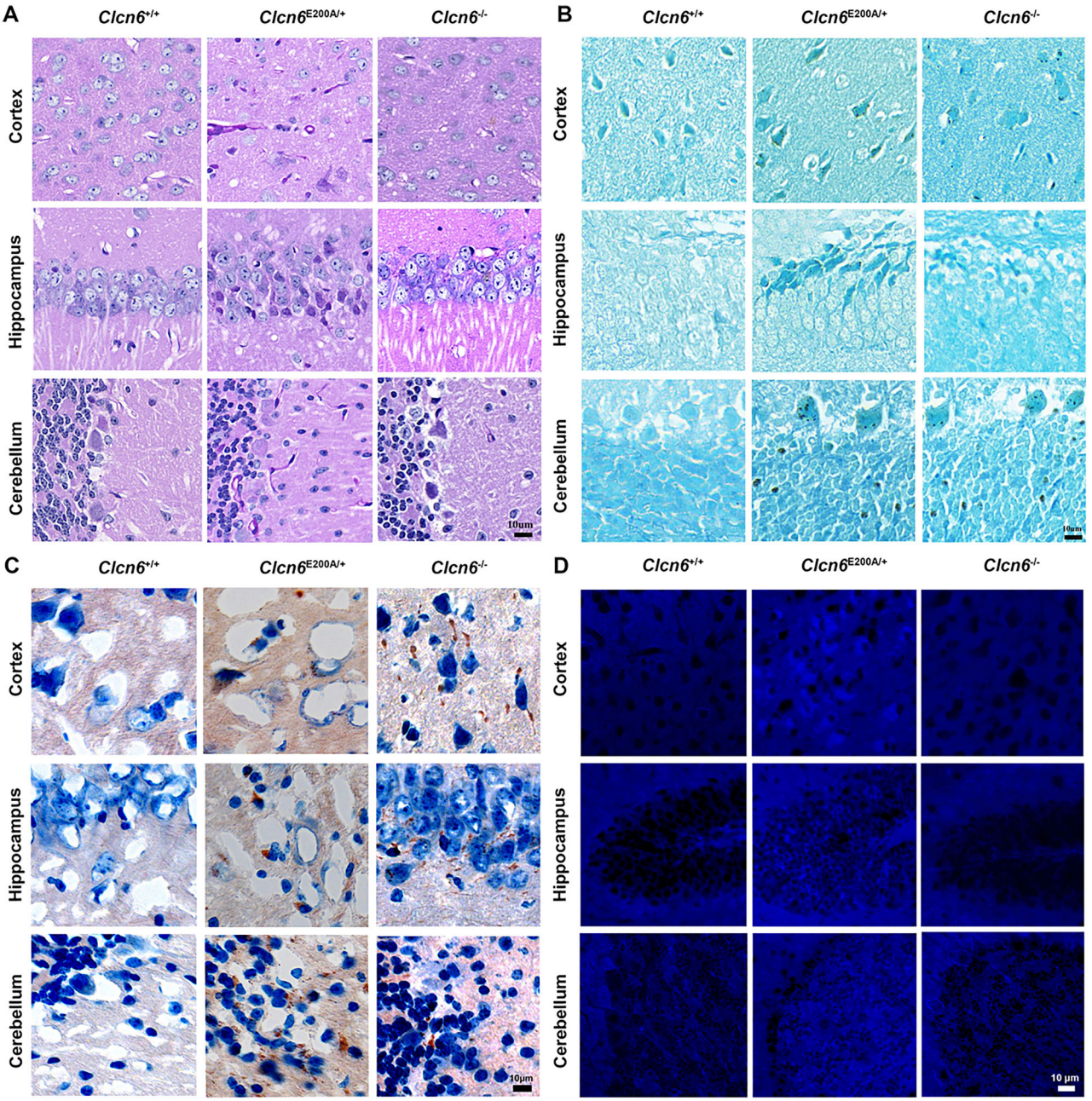


**FIGURE 6: Metabolic disorder in the brain of *Clcn6*$^{E200A/+}$ and *Clcn6*$^{-/-}$ mice. (A) PAS staining of paraffin-embedded brain sections revealed accumulation of carbohydrates in the intercellular space of the cortex (representative images of the primary motor cortex) and cerebellum, and in the neuronal perikaryon of the hippocampus of 5-month-old *Clcn6*$^{E200A/+}$ mice, but not in *Clcn6*$^{-/-}$ mice. (B) Luxol fast blue staining for lipofuscin revealed granular deposits in most neuronal somata, particularly in Purkinje and granule cells of the cerebellum, of 5-month-old *Clcn6*$^{E200A/+}$ and *Clcn6*$^{-/-}$ mice. For the cortex, representative images of the primary motor cortex are shown. (C) Oil Red O staining revealed the existence of massive red-stained lipids in neurons of the cortex (representative images of the secondary visual cortex, mediolat), hippocmpus and cerebellum of both 5-month-old *Clcn6*$^{E200A/+}$ and *Clcn6*$^{-/-}$ mice. (D) Filipin staining showed more unesterified cholesterol in the cortex (representative images of the primary motor cortex), hippocampus and cerebellum of 5-month-old *Clcn6*$^{E200A/+}$ mice than in age-matched WT or *Clcn6*$^{-/-}$ mice. Scale bars: 10 μm.**

*Clcn6*$^{E200A/+}$ and *Clcn6*$^{-/-}$ mice. Luxol fast blue staining for lipofuscin[20] revealed granular deposits in most neuronal somata, particularly in Purkinje and granule cells of the cerebellum, of 5-month-old *Clcn6*$^{E200A/+}$ and *Clcn6*$^{-/-}$ (Fig 6B). Additionally, Oil Red O staining revealed massive lipid accumulation in neurons of the cortex, hippocampus, cerebellum of both 5-month-old *Clcn6*$^{E200A/+}$ and *Clcn6*$^{-/-}$ mice (Fig 6C). As expected, and consistent with our in vitro data (Fig 2D), 5-month-old *Clcn6*$^{E200A/+}$ mice had more unesterified cholesterol in the cortex, hippocampus, cerebellum than age-matched WT or *Clcn6*$^{-/-}$ mice, as shown by Filipin staining (Fig 6D). Taken together, these results demonstrate that glycometabolism and lipid metabolism disorder were evident in *Clcn6*$^{E200A/+}$ brain, while only lipid metabolism was disrupted in *Clcn6*$^{-/-}$ brain.

### Increased Protein Levels of ClC-6$^{E200A}$, but Not of Other Vesicular CLCs in Clcn6$^{E200A/+}$ Brain

For ClC-6, we found markedly increased protein levels in all examined brain regions of P120 *Clcn6*$^{E200A/+}$ mice compared to WT mice (Figs 7A and S20). Notably, for newborn mice (postnatal day 0 [P0]), no significant differences in ClC-6 levels were observed between WT and *Clcn6*$^{E200A/+}$ brain (Fig S21), which shows that accumulation of mutant ClC-6 protein occurs only later. As expected, ClC-6 protein was not detectable in liver of each genotype, or in brain tissues of *Clcn6*$^{-/-}$ mice (Figs 7A, S20 and S21). The increase of ClC-6 levels in the brain of 4-month-old *Clcn6*$^{E200A/+}$ mice was not due to increased gene transcription as quantitative real-time polymerase chain reaction (qRT-PCR) revealed unchanged *Clcn6* mRNA levels compared with WT controls (Fig S22).

The strikingly more severe phenotype in *Clcn6*$^{E200A/+}$ mice compared to *Clcn6*$^{-/-}$ mice could be explained by the possibility that other vesicular CLC proteins might compensate for a loss of ClC-6 function in *Clcn6*$^{-/-}$, but not in *Clcn6*$^{E200A/+}$ mice. However, immunoblot examination of the protein levels of the ClC-6 paralogs expressed in brain revealed unchanged protein levels of ClC-3, ClC-4 and ClC-7 in *Clcn6*$^{E200A/+}$ and *Clcn6*$^{-/-}$ P0 brains (Fig S21).

### Early and Progressive Lysosomal Impairments in Clcn6$^{E200A/+}$ Brain

To evaluate lysosomal function, we first analyzed the expression levels of cathepsin D (CTSD) and lysosomal-associated membrane protein 1 (Lamp1). Compared to WT control brains, the levels of pro-CTSD and Lamp1 were increased in *Clcn6*$^{E200A/+}$ mice at P35 (Fig S23), a time when the overall cellular morphology appeared normal but neurons were already dysfunctional, and further increased in all tested brain areas at P120 *Clcn6*$^{E200A/+}$ brain (Figs 7A and S20). We also observed increased levels of mature-CTSD in all tested brain areas at P120 *Clcn6*$^{E200A/+}$ brain (Figs 7A and S20). However, we did not find any differences among the 3 genotypes at asymptomatic age (P0) (Figs 7B and S24). These abnormalities in CTSD and Lamp1 levels were not observed in *Clcn6*$^{-/-}$ mice at all ages tested, regardless of the brain regions examined (Figs 7A,B, S20, S23, and S24). As expected, CTSD and Lamp1 levels were not altered in the liver of P120 *Clcn6*$^{E200A/+}$ and *Clcn6*$^{-/-}$ mice (Figs 7A,B and S20). Immunohistochemistry confirmed the increase of CTSD in cortex, hippocampus, and cerebellum of 4-month-old *Clcn6*$^{E200A/+}$ mice (Fig 7C). While total protein levels of CTSD were unchanged in P120 *Clcn6*$^{-/-}$ brain, immunohistochemistry revealed that CTSD was concentrated in proximal axons and strongly reduced in somata of 4-month-old *Clcn6*$^{-/-}$ brain (Fig 7C). However, the enzymatic activity of CTSD was not significantly altered in the cortex of *Clcn6*$^{E200A/+}$ or *Clcn6*$^{-/-}$ mice at 5 months (Fig S25). Overall, these results hint at an early and progressive impairment in lysosomal function in the *Clcn6*$^{E200A/+}$ brain.

### Early and Progressive Autophagy Defects in Clcn6$^{E200A/+}$ Brain

Consistent with the effect of ectopically expressed ClC-6 variants in HeLa cells (Figs 2A and S1), the LC3-II/LC3-I ratio was significantly increased in the brain of *Clcn6*$^{E200A/+}$ mice at P35 (Fig S23) in comparison to WT, and further increased in all tested brain areas of *Clcn6*$^{E200A/+}$ mice at P120 (Figs 7A, and S20). This was accompanied by a significant increase in the autophagy substrate protein SQSTM/p62 (Figs 7A and S20 and S23). In contrast, the LC3-II/LC3-I ratio and the SQSTM1/p62 levels were unchanged at P0 (Figs 7B and S24). Altogether, the gradual accumulation of LC3-II and SQSTM1/p62 suggests a lysosomal dysfunction in neurons of *Clcn6*$^{E200A/+}$ mice leading to an accumulation of autophagosomes. Conversely, there was no substantial difference in the LC3-II/LC3-I ratio or the SQSTM1/p62 levels between *Clcn6*$^{-/-}$ and WT brains at any age (Figs 7A,B, S20, S23, and S24). In addition, immunohistochemistry analyses showed strong staining of SQSTM1/p62 in many brain regions of *Clcn6*$^{E200A/+}$ mice at 4 months, but not age-matched WT or *Clcn6*$^{-/-}$ mice (Fig 7D). Moreover, we observed higher levels of mitochondrial ATP synthase subunit c (SCMAS) immunoreactivity in various brain regions of P100 *Clcn6*$^{E200A/+}$ mice than in WT controls, whereas SCMAS immunoreactivity in the *Clcn6*$^{-/-}$ brain was concentrated in proximal axons (Fig 7E). Consistent with the immunohistochemistry

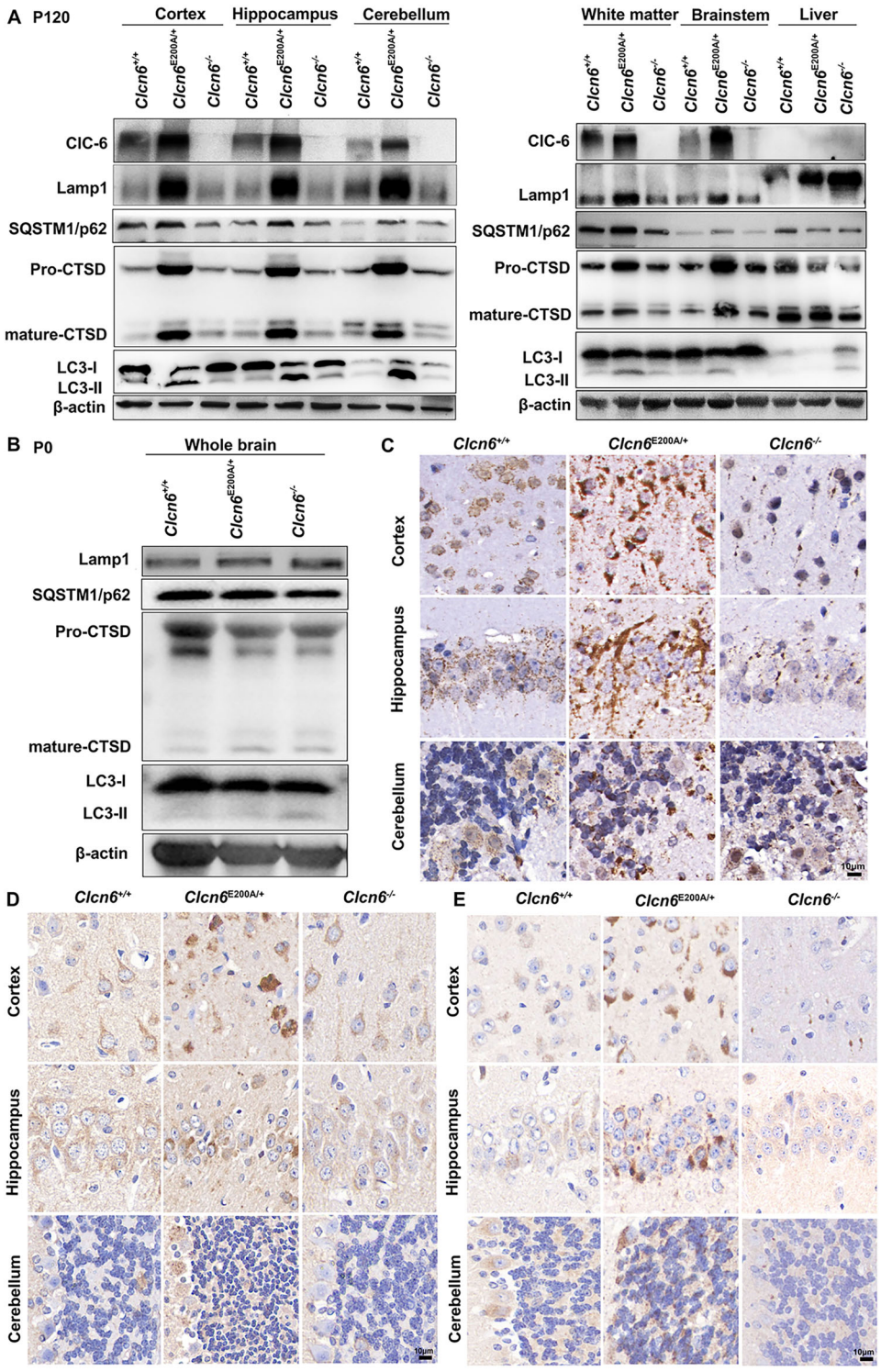


FIGURE 7: Lysosomal function and autophagy in *Clcn6*$^{E200A/+}$ mice. (A) Western blot analysis showed an increase of ClC-6, Lamp1, pro-CTSD, mature-CTSD, SQSTM1/p62, and LC3-II/ LC3-I in the cortex, hippocampus, cerebellum, white matter, and brainstem from P120 *Clcn6*$^{E200A/+}$ mice compared to WT littermates. For quantification, see Figure S20. (B) No change of ClC-6, Lamp1, pro-CTSD, mature-CTSD, SQSTM1/p62, and LC3-II/ LC3-I in total brain extracts of *Clcn6*$^{E200A/+}$ mice, compared to WT littermates at P0. For quantification, see Figure S24. (C) Intense immunostaining for CTSD was localized to neuronal perikarya in 4-month-old *Clcn6*$^{E200A/+}$ mice, whereas mild immunoreactivity is only detected in the in the proximal axon of age matched *Clcn6*$^{-/-}$ mice. (D) Immunohistochemical staining showing SQSTM1/p62-positive aggregates in the cortex, hippocampus, and cerebellum from 5-month-old *Clcn6*$^{E200A/+}$ mice, compared to age-matched WT or *Clcn6*$^{-/-}$ mice. (E) Immunostaining for SCMAS is large-granular and intensely localized to neuronal perikarya in P100 *Clcn6*$^{E200A/+}$ mice, whereas mild immunoreactivity is only detected in the in the proximal axon of P100 *Clcn6*$^{-/-}$ mice. (C-E) For the cortex, representative images of the primary motor cortex are shown. Scale bars: 10 μm.

studies, Western blot analysis showed an increase of SCMAS in total brain extracts of *Clcn6*$^{E200A/+}$ mice at 5 months, compared to age-matched WT or *Clcn6*$^{-/-}$ mice (Fig S26). These data imply impairment of autophagy of mitochondria (mitophagy) in the brain of *Clcn6*$^{E200A/+}$ mice. Collectively, our data show that autophagy defects are early pathogenic events in the *Clcn6*$^{E200A/+}$ brain preceding neurodegeneration.

### *Altered mTOR-TFEB Signaling in Clcn6$^{E200A/+}$ Brain*

Overexpression of ClC-6$^{E200A}$ or ClC-6$^{Y553C}$ activated TFEB (Fig 2B). Therefore, we assessed the expression of TFEB target genes, including autophagy (*Lc3b*, *Sqtm1/p62*, *Vps8*, *Vps11*, and *Uvrag*) and lysosomal (*Lamp1*, *Cln3*, *Wipi*, *Ctsa, Ctsb*, *Ctsd*, *Ctsf*, *Atp6v1h*, and *Clcn7*) genes in the brains of 4-to-5-month-old WT, *Clcn6*$^{E200A/+}$

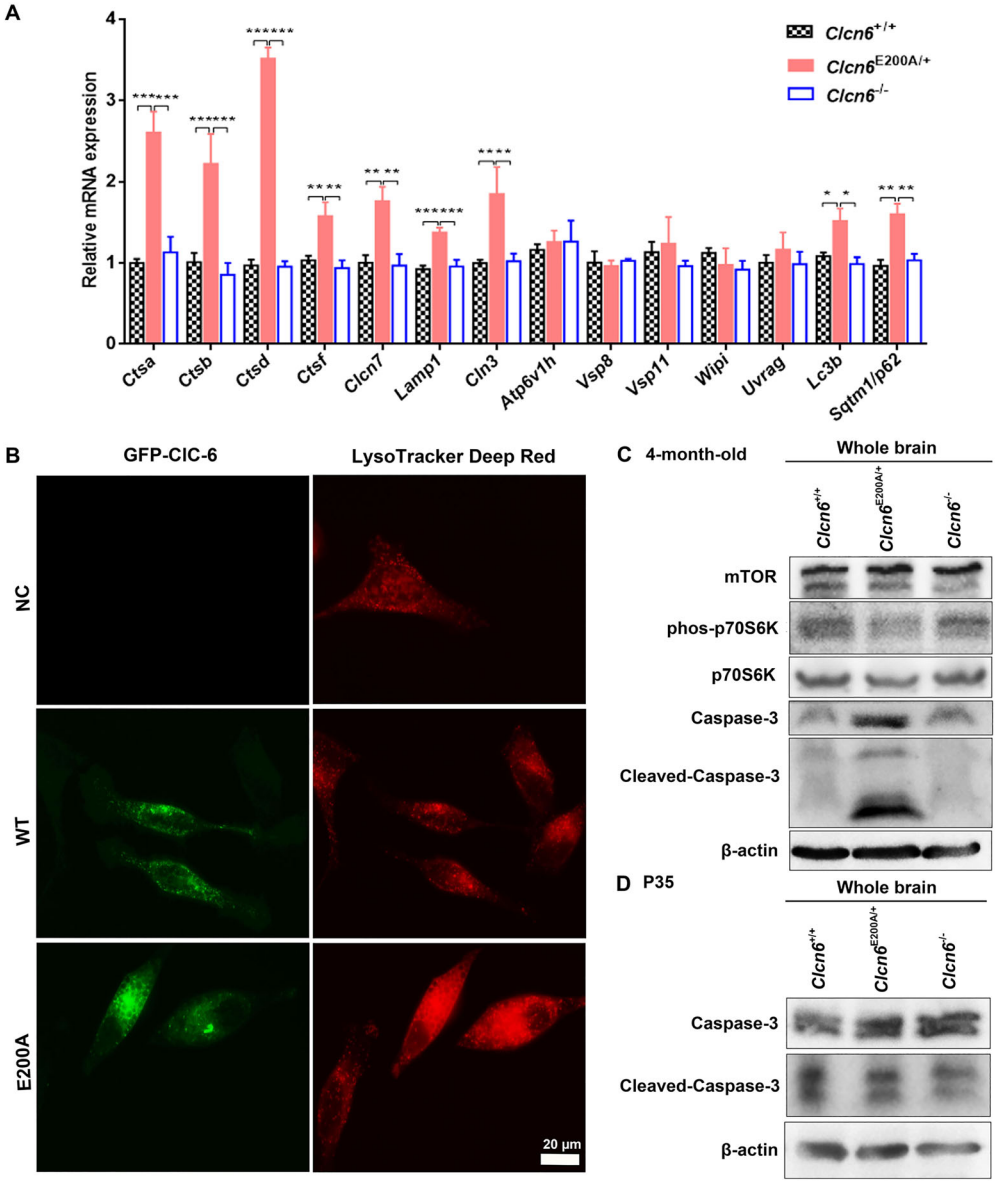


**FIGURE 8: mTORC1-TFEB signaling pathway and apoptosis in *Clcn6*$^{E200A/+}$ brain. (A) The levels of lysosomal and autophagic gene mRNA in brain samples of 4- to 5-month-old WT, *Clcn6*$^{E200A/+}$, and *Clcn6*$^{-/-}$ mice were quantified by qRT-PCR and normalized to *Gapdh*. (B) HeLa cells transfected with either WT or p.E200A mutant ClC-6 and stained with LysoTracker Deep Red. The fluorescence intensity and size of LysoTracker-stained acidic vesicles in ClC-6 p.E200A-expressing cells is increased compared with ClC-6 WT-expressing cells. Scale bar: 20 μm. For quantification, see Figure S27. (C) Western blot analysis of mTOR, phos-p70S6K, p70S6K, caspase-3, and cleaved-Caspase-3 of total brain homogenates from 4-month-old *Clcn6*$^{E200A/+}$, *Clcn6*$^{-/-}$, and WT mice. For quantification, see Figure S28. (D) No change of caspase-3 and cleaved-Caspase-3 in total brain extracts of *Clcn6*$^{E200A/+}$ mice, compared to WT littermates at P35. For quantification, see Figure S29. [Color figure can be viewed at www.annalsofneurology.org]**

and *Clcn6*$^{-/-}$ mice. qRT-PCR revealed an increase in mRNA levels of many lysosomal genes, including some orthologs of human NCL genes (*CLN3*, *CLN10/CTSD*, and *CLN13/CTSF*), and of some autophagic genes (*Lc3Bb*, *Sqtm1/p62*) in *Clcn6*$^{E200A/+}$ mice compared to their WT littermates (Fig 8A). In contrast, there was no difference in the mRNA levels of lysosomal or autophagic genes in brain of *Clcn6*$^{-/-}$ mice (Fig 8A). Consistent with increased lysosomal biogenesis in the presence of ClC-6$^{E200A}$, we observed a significant increase in the number and size of LysoTracker-stained acidic vesicles in cells ectopically expressing ClC-6$^{E200A}$, compared to WT ClC-6-transfected cells (Figs 8B and S27).

As TFEB activity is regulated by the kinase mTORC1, we tested for mTORC1 activity. We found significantly reduced levels of phosphorylated p70S6K, a major mTORC1 target, in brain extracts of 4-month-old *Clcn6*$^{E200A/+}$ mice, compared to those of WT and *Clcn6*$^{-/-}$ mice (Figs 8C and S28). The reduction in mTORC1 activity was not due to decreased protein level as no change in mTOR protein levels was detected in *Clcn6*$^{E200A/+}$ brain (Figs 8C and S28).

Taken together, these data suggest that the activity of mTORC1 is reduced in *Clcn6*$^{E200A/+}$, leading to increased TFEB activity, which in turn results in increased lysosomal size and number.

### *Neuronal Apoptosis in* Clcn6$^{E200A/+}$ *Brain*

Last, we tested for an involvement of apoptosis in the neuronal degeneration in *Clcn6*$^{E200A/+}$ mice. Procaspase-3 and cleaved caspase-3 were markedly elevated in 4-month-old *Clcn6*$^{E200A/+}$ mice, compared to WT or *Clcn6*$^{-/-}$ counterparts (Figs 8C and S28). However, procaspase-3 and cleaved caspase-3 showed no differences among the 3 genotypes at P35 (Figs 8D and S29). These results indicate that apoptosis occurs only at later stages in *Clcn6*$^{E200A/+}$ mice.

## Discussion

In this study, we describe a girl with a de novo *CLCN6* p.E200A variant, who presented intractable epilepsy, progressive cognitive decline, motor impairment, behavioral abnormities, retinal dysfunction, and progressive brain atrophy, suggestive of NCLs. Moreover, we characterized the first *Clcn6* knock-in mouse model harboring a heterozygous disease-associated *Clcn6* variant. Heterozygous *Clcn6*$^{E200A/+}$ mice developed severe neurological phenotypes including tremor, seizures, ataxia, visual impairment, behavioral abnormalities, and premature death, all together resembling human NCLs.[21–23] *Clcn6*$^{E200A/+}$ mice also developed a number of neuropathological features similar to those that occur in NCLs,[21,22] including a massive accumulation of SCMAS and autofluorescent lipopigment, brain atrophy, progressive neuron loss, defective myelination as well as progressive glial activation. So, our study shows that the *Clcn6*$^{E200A/+}$ mutant mouse model displays many phenotypic similarities to the patient with the equivalent *CLCN6* variant, and recapitulates virtually all characteristic clinical and pathological features of human NCLs.

NCLs are a devastating subclass of genetic lysosomal storage diseases (LSDs) which manifest in early childhood.[21] So far, 13 different NCL genes (*CLN1-8,10–14*) have been identified, many of which encode proteins in the endosomal/lysosomal pathway.[22–26] The existence of patients with NCL-like pathology but no mutation in any of these genes suggests additional unknown NCL genes.[27] Patients with the heterozygous *CLCN6* p.E200A variant as well as 3 patients carrying a heterozygous *CLCN6* p.Y553C variant and 1 patient with the p.T520A variant showed progressive cognitive decline, motor deficiencies, visual impairment, and developmental regression,[4,6,8] symptoms strikingly resembling those seen in NCL patients. Expression of ClC-6$^{E200A}$ or ClC-6$^{Y553C}$ mutants in HeLa cells impaired the lysosomal degradation of autophagic material, and led to free cholesterol accumulation, indicating disease-causing ClC-6 mutants cause a kind of metabolic disorders, such as LSDs. Our *Clcn6*$^{E200A/+}$ mice phenocopied the *CLCN6* p.E200A patients, and the *Clcn6*$^{E200A/+}$ brain pathology mirrored the pathology of human NCLs. Altogether, this study demonstrates that *CLCN6* is a novel gene for NCLs and indicates that *CLCN6* should be considered in the diagnostic workup for molecularly undefined forms of NCLs.

There is a striking difference between the clinical features and symptoms found in human with *CLCN6* disease-causing mutations and *Clcn6*$^{E200A/+}$ mice on the one side and the much milder phenotype in *Clcn6*$^{-/-}$ mice,[3] which was reproduced in this study, on the other side (Table S2). *Clcn6*$^{-/-}$ mice only displayed mild behavioral abnormalities from 3 to 5 months of age.[3] Their brains showed no prominent brain atrophy or obvious neuron loss, despite marked autofluorescence in proximal axons, which were often ballooned and contained lysosomal storage material.[3] Unexpectedly, our analyses showed previously unrecognized ventricle dilation and retinal dysfunction in *Clcn6*$^{-/-}$ mice. Nonetheless, the overall absence of an obvious neurological phenotype and neuron loss in *Clcn6*$^{-/-}$ mice demonstrates that ClC-6 loss-of-function only mildly impinges on neuronal function. In addition, the ClC-6$^{E200A}$ mutant suppressed mTORC1 activity, enhanced TFEB and TFE3 translocation and up-regulated expression of autophagic-lysosomal genes, whereas deletion of ClC-6 did not cause such changes. Therefore, these data suggest that the p.E200A

mutation causes toxicity by a gain-of-function, similar to the p.Y553C mutation[6] and consistent with the dominant phenotype in the heterozygous patients and animals. The p.Y553C mutant mediates larger currents especially at lower extracytosolic pH.[6,9] A gain-of-function by the p.E200A mutation, despite its uncoupling of anion transport from proton antiport, may be explained by the loss of rectification that allows $Cl^-$ transport at voltages where the rectifying exchanger mediates less currents.[10]

The severe consequences of the heterozygous p.E200A variant in the patients and in the mouse model are also intriguing in respect to the equivalent mouse models for CLC paralogs. Mutations in all of the neuronal CLC $Cl^-/H^+$ exchangers ClC-3, −4, −6, and − 7 underlie a spectrum of neurological disorders.[4,6,15,28–32] Mouse models lacking the endosomal ClC-3 or the lysosomal ClC-7 develop neurodegeneration.[33–37] The complete substitution of the respective $Cl^-/H^+$ exchanger, in the background of ClC-4-deficiency in the case of ClC-3, by its gating glutamate mutant that uncouples chloride from proton transport results in virtually the same phenotype as its knock-out. However, mice heterozygous for such mutation in *Clcn3* or *Clcn7* do not present obvious phenotypes.[12,13] Likewise, mice[11] and patients[14,38] with uncoupled ClC-5 display virtually the same phenotype as observed with a loss of ClC-5 function.[39] It remains to be determined why the gating glutamate mutation in ClC-6 has a dominant effect that is not found in the other vesicular CLCs.

Electron microscopy studies showed an accumulation of lipid droplets and lipofuscin in the neuronal soma and axon of *Clcn6*$^{E200A/+}$ mice, whereas this storage material was present predominantly in the proximal axon of *Clcn6*$^{-/-}$ mice. In histochemistry, the storage material in *Clcn6*$^{E200A/+}$ brain was strongly autofluorescent, positive for Luxol-fast blue, Oil red O, and Filipin, and distributed in the perikaryon. In contrast, the storage material in *Clcn6*$^{-/-}$ brain was strongly autofluorescent, only positive for Luxol-fast blue, Oil red O, but negative for Filipin. Lipidomic studies are needed to determine the exact nature of the lipids stored in the *Clcn6*$^{E200A/+}$ and *Clcn6*$^{-/-}$ neurons. In addition, we observed PAS-positive granular deposits in the perikaryon of neurons, and in the intercellular space of cortex, hippocampus, and cerebellum of 5-month-old *Clcn6*$^{E200A/+}$ mice, whereas such PAS staining was not detected in age-matched *Clcn6*$^{-/-}$ brain. Collectively, these data suggest that a lipid metabolism disorder may contribute to the common neuropathology in both *Clcn6*$^{E200A/+}$ and *Clcn6*$^{-/-}$ mice, which ultimately leads to myelination defects. By contrast, the disturbance of glycometabolism may be associated with more severe neuropathology in *Clcn6*$^{E200A/+}$ mice. Therefore, regulating lipid metabolism and glycometabolism may be a therapeutic option for the treatment of *CLCN6*-related NCLs.

The autophagic-lysosomal pathway is a critical cellular quality control system. Its disturbance has been recognized as a major pathomechanism contributing to the accumulation of storage material and neurodegeneration in various neurodegenerative diseases including several NCLs.[24,40–42] The accumulation of autophagic vacuoles and the age-dependent increase in autophagic marker proteins suggest that the autophagic degradation pathway is impaired in the brain of *Clcn6*$^{E200A/+}$ mice. While not detectable in newborn mice, autophagic defects developed with the time of lysosomal dysfunction, in agreement with a contribution of autophagy defects to the initiation of neuron loss in *Clcn6*$^{E200A/+}$ mice.

The accumulation of autophagic vacuoles in *Clcn6*$^{E200A/+}$ mice is likely due to impaired clearance secondary to lysosome dysfunction, as we previously found reduced autophagosome-lysosome fusion in ClC-6$^{E200A}$-expressing cells.[4] Accumulation of storage material upon lysosomal dysfunction, which we find in *Clcn6*$^{E200A/+}$ mice, triggers mTORC1-TFEB/TFE3 signaling leading to enhanced lysosomal biogenesis.[43–45] Consistently, mTORC1 activity was decreased in mouse brains and various lysosomal proteins. Their mRNA levels showed an age-dependent increase in *Clcn6*$^{E200A/+}$ mouse brain. Overexpression of disease-causing p.E200A and p.Y553C ClC-6 mutants induced TFEB and TFE3 nuclear translocation in HeLa cells as well. Increased Lamp1 and CTSD levels were detected in P35 *Clcn6*$^{E200A/+}$ brains, many days before obvious neuron loss, indicating that lysosomal dysfunction is an early event in *Clcn6*$^{E200A/+}$ neuropathology. *Clcn6*$^{E200A/+}$ mice also prominently featured early detectable, widespread astrogliosis and microgliosis. It is unclear whether glial activation directly promotes neuronal cell loss, or presents a secondary, but easily detectable consequence of the disease process.

In summary, we described a girl with a de novo *CLCN6* p.E200A variant, who presented a range of neurological defects that are suggestive of NCLs. The *Clcn6*$^{E200A/+}$ mouse model, the first one with a human disease-causing ClC-6 variant, demonstrates the importance of $Cl^-/H^+$-exchange activity for ClC-6 function. It phenocopies the *CLCN6* p.E200A patients, and clinically and pathologically fulfills the characteristics of human NCLs. Therefore, our work establishes variants in *CLCN6* as a novel genetic cause of NCLs via gain-of-function toxicity, highlighting the importance of considering *CLCN6* mutations in the diagnosis of NCLs. Our study reveals a role of altered mTORC1-TFEB/TFE3 signaling and autophagy-lysosome function, the disturbance of lipid metabolism and glycometabolism, and apoptosis in ClC-

6-mediated NCLs. We also present the sequence of pathogenic events in neurodegenerating *Clcn6*$^{E200A/+}$ brains, with autophagic dysfunction, lysosome deficiency, and gliosis being early events leading to neuronal dysfunction. This is helpful for both understanding the molecular mechanism of NCLs and developing therapeutic treatments of related neurodegenerative disorders.

## Conclusion

*CLCN6* variants interfere with the TFEB/TFE3 axis of mTORC1 signaling via a dominant effect, and cause NCLs. Moreover, $Cl^-/H^+$-exchange activity is critical to the physiological function of ClC-6.


## Acknowledgments

We thank the patient and her parents for participating in this study. We also thank Tenghui Wu, Renbin Lu, and Jieqiong Tan for technical assistance. The project was supported by grants from the National Natural Science Foundation of China (82071462 and 81771409 to P.J.; 82201316 to H.H.), the China Postdoctoral Science Foundation (2023 M733950 to H.H.), the Natural Science Foundation of Hunan Province (2022JJ40785 to H. H.), the Key Research and Deleopment Program of Hunan Province (2022SK2036 to P.J.), the German Research Foundation (DFG) within FOR2625 (JE 164/14-2 to T.J.J.; STA 1543/1-2 to T.S.), and a China Scholarship Council fellowship to H.H. The publication was supported by the Open Access Fund of the MSH Medical School Hamburg. Open Access funding enabled and organized by Projekt DEAL.


## Author Contributions

H.H., T.S., and J.P. contributed to the conception and design of the study; all authors contributed to the acquisition and analysis of data; H.H., T.J.J., T.S., and J.P. contributed to drafting the text or preparing the figures. All authors approved the final version of the manuscript.

## Potential Conflicts of Interest

Nothing to report.

### *Data availability*

All data needed to evaluate the conclusions are present in the paper and/or the Supplementary Materials.

## References


1. Jentsch TJ, Pusch M. CLC chloride channels and transporters: structure, function, physiology, and disease. Physiol Rev 2018; 98:1493–1590. https://doi.org/10.1152/physrev.00047.2017.
2. Brandt S, Jentsch TJ. ClC-6 and ClC-7 are two novel broadly expressed members of the CLC chloride channel family. FEBS Lett 1995;377:15–20. https://doi.org/10.1016/0014-5793(95)01298-2.
3. Poët M, Kornak U, Schweizer M, et al. Lysosomal storage disease upon disruption of the neuronal chloride transport protein ClC-6. Proc Natl Acad Sci U S A 2006;103:13854–13859. https://doi.org/10.1073/pnas.0606137103.
4. He H, Cao X, Yin F, et al. West syndrome caused by a chloride/proton exchange-uncoupling *CLCN6* mutation related to autophagic-lysosomal dysfunction. Mol Neurobiol 2021;58:2990–2999. https://doi.org/10.1007/s12035-021-02291-3.
5. Peng J, Wang Y, He F, et al. Novel West syndrome candidate genes in a Chinese cohort. CNS Neurosci Ther 2018;24:1196–1206. https://doi.org/10.1111/cns.12860.
6. Polovitskaya MM, Barbini C, Martinelli D, et al. A recurrent gain-of-function mutation in *CLCN6*, encoding the ClC-6 $Cl^-/H^+$-exchanger, causes early-onset neurodegeneration. Am J Hum Genet 2020;107:1062–1077. https://doi.org/10.1016/j.ajhg.2020.11.004.
7. Wang Y, Du X, Bin R, et al. Genetic variants identified from epilepsy of unknown etiology in Chinese children by targeted exome sequencing. Sci Rep 2017;7:40319. https://doi.org/10.1038/srep40319.
8. Zhang B, Zhang S, Polovitskaya MM, et al. Molecular basis of ClC-6 function and its impairment in human disease. Sci Adv 2023;9: eadg4479. https://doi.org/10.1126/sciadv.adg4479.
9. Zifarelli G, Pusch M, Fong P. Altered voltage-dependence of slowly activating chloride-proton antiport by late endosomal ClC-6 explains distinct neurological disorders. J Physiol 2022;600:2147–2164. https://doi.org/10.1113/JP282737.
10. Neagoe I, Stauber T, Fidzinski P, et al. The late endosomal ClC-6 mediates proton/chloride countertransport in heterologous plasma membrane expression. J Biol Chem 2010;285:21689–21697. https://doi.org/10.1074/jbc.M110.125971.
11. Novarino G, Weinert S, Rickheit G, Jentsch TJ. Endosomal chloride-proton exchange rather than chloride conductance is crucial for renal endocytosis. Science 2010;328:1398–1401. https://doi.org/10.1126/science.1188070.
12. Weinert S, Gimber N, Deuschel D, et al. Uncoupling endosomal CLC chloride/proton exchange causes severe neurodegeneration. EMBO J 2020;39:e103358. https://doi.org/10.15252/embj.2019103358.
13. Weinert S, Jabs S, Supanchart C, et al. Lysosomal pathology and osteopetrosis upon loss of $H^+$-driven lysosomal $Cl^-$ accumulation. Science 2010;328:1401–1403. https://doi.org/10.1126/science.1188072.
14. Bignon Y, Alekov A, Frachon N, et al. A novel *CLCN5* pathogenic mutation supports dent disease with normal endosomal acidification. Hum Mutat 2018;39:1139–1149. https://doi.org/10.1002/humu.23556.
15. He H, Guzman RE, Cao D, et al. The molecular and phenotypic spectrum of *CLCN4*-related epilepsy. Epilepsia 2021;62:1401–1415. https://doi.org/10.1111/epi.16906.
16. Martina JA, Diab HI, Lishu L, et al. The nutrient-responsive transcription factor TFE3 promotes autophagy, lysosomal biogenesis, and clearance of cellular debris. Sci Signal 2014;7:ra9. https://doi.org/10.1126/scisignal.2004754.
17. Sardiello M, Palmieri M, di Ronza A, et al. A gene network regulating lysosomal biogenesis and function. Science 2009;325:473–477. https://doi.org/10.1126/science.1174447.

18. Settembre C, Di Malta C, Polito VA, et al. TFEB links autophagy to lysosomal biogenesis. Science 2011;332:1429–1433. https://doi.org/10.1126/science.1204592.

19. Takahashi K, Eultgen E, Wang S, et al. Gene therapy ameliorates spontaneous seizures associated with cortical neuron loss in a *Cln2*$^{R207X}$ mouse model. J Clin Invest 2023;133:e165908. https://doi.org/10.1172/JCI165908.

20. Bronson RT, Donahue LR, Johnson KR, et al. Neuronal ceroid lipofuscinosis (*ncl*f), a new disorder of the mouse linked to chromosome 9. Am J Med Genet 1998;77:289–297. https://doi.org/10.1002/(sici)1096-8628(19980526)77:4<289::AID-AJMG8>3.0.CO;2-I.

21. Johnson TB, Cain JT, White KA, et al. Therapeutic landscape for Batten disease: current treatments and future prospects. Nat Rev Neurol 2019;15:161–178. https://doi.org/10.1038/s41582-019-0138-8.

22. Kaminiów K, Kozak S, Paprocka J. Recent insight into the genetic basis, clinical features, and diagnostic methods for neuronal ceroid lipofuscinosis. Int J Mol Sci 2022;23:5729. https://doi.org/10.3390/ijms23105729.

23. Mole SE, Anderson G, Band HA, et al. Clinical challenges and future therapeutic approaches for neuronal ceroid lipofuscinosis. Lancet Neurol 2019;18:107–116. https://doi.org/10.1016/S1474-4422(18)30368-5.

24. Mukherjee AB, Appu AP, Sadhukhan T, et al. Emerging new roles of the lysosome and neuronal ceroid lipofuscinoses. Mol Neurodegener 2019;14:4. https://doi.org/10.1186/s13024-018-0300-6.

25. Williams RE, Mole SE. New nomenclature and classification scheme for the neuronal ceroid lipofuscinoses. Neurology 2012;79:183–191. https://doi.org/10.1212/WNL.0b013e31825f0547.

26. Kollmann K, Uusi-Rauva K, Scifo E, et al. Cell biology and function of neuronal ceroid lipofuscinosis-related proteins. Biochim Biophys Acta 2013;1832:1866–1881. https://doi.org/10.1016/j.bbadis.2013.01.019.

27. Di Fruscio G, Schulz A, De Cegli R, et al. Lysoplex: an efficient toolkit to detect DNA sequence variations in the autophagy-lysosomal pathway. Autophagy 2015;11:928–938. https://doi.org/10.1080/15548627.2015.1043077.

28. Bose S, He H, Stauber T. Neurodegeneration upon dysfunction of endosomal/lysosomal CLC chloride transporters. Front Cell Dev Biol 2021;9:639231. https://doi.org/10.3389/fcell.2021.639231.

29. Duncan AR, Polovitskaya MM, Gaitán-Peñas H, et al. Unique variants in *CLCN3*, encoding an endosomal anion/proton exchanger, underlie a spectrum of neurodevelopmental disorders. Am J Hum Genet 2021;108:1450–1465. https://doi.org/10.1016/j.ajhg.2021.06.003.

30. Palmer EE, Pusch M, Picollo A, et al. Functional and clinical studies reveal pathophysiological complexity of *CLCN4*-related neurodevelopmental condition. Mol Psychiatry 2022;28:668–697. https://doi.org/10.1038/s41380-022-01852-9.

31. Palmer EE, Stuhlmann T, Weinert S, et al. De novo and inherited mutations in the X-linked gene *CLCN4* are associated with syndromic intellectual disability and behavior and seizure disorders in males and females. Mol Psychiatry 2018;23:222–230. https://doi.org/10.1038/mp.2016.135.

32. Nicoli ER, Weston MR, Hackbarth M, et al. Lysosomal storage and albinism due to effects of a de novo *CLCN7* variant on lysosomal acidification. Am J Hum Genet 2019;104:1127–1138. https://doi.org/10.1016/j.ajhg.2019.04.008.

33. Dickerson LW, Bonthius DJ, Schutte BC, et al. Altered GABAergic function accompanies hippocampal degeneration in mice lacking ClC-3 voltage-gated chloride channels. Brain Res 2002;958:227–250. https://doi.org/10.1016/s0006-8993(02)03519-9.

34. Kasper D, Planells-Cases R, Fuhrmann JC, et al. Loss of the chloride channel ClC-7 leads to lysosomal storage disease and neurodegeneration. EMBO J 2005;24:1079–1091. https://doi.org/10.1038/sj.emboj.7600576.

35. Pressey SN, O'Donnell KJ, Stauber T, et al. Distinct neuropathologic phenotypes after disrupting the chloride transport proteins ClC-6 or ClC-7/Ostm1. J Neuropathol Exp Neurol 2010;69:1228–1246. https://doi.org/10.1097/NEN.0b013e3181ffe742.

36. Stobrawa SM, Breiderhoff T, Takamori S, et al. Disruption of ClC-3, a chloride channel expressed on synaptic vesicles, leads to a loss of the hippocampus. Neuron 2001;29:185–196. https://doi.org/10.1016/s0896-6273(01)00189-1.

37. Yoshikawa M, Uchida S, Ezaki J, et al. CLC-3 deficiency leads to phenotypes similar to human neuronal ceroid lipofuscinosis. Genes Cells 2002;7:597–605. https://doi.org/10.1046/j.1365-2443.2002.00539.x.

38. Sekine T, Komoda F, Miura K, et al. Japanese Dent disease has a wider clinical spectrum than Dent disease in Europe/USA: genetic and clinical studies of 86 unrelated patients with low-molecular-weight proteinuria. Nephrol Dial Transplant 2014;29:376–384. https://doi.org/10.1093/ndt/gft394.

39. Piwon N, Günther W, Schwake M, et al. ClC-5 $Cl^-$ channel disruption impairs endocytosis in a mouse model for Dent's disease. Nature 2000;408:369–373.

40. Nelvagal HR, Lange J, Takahashi K, et al. Pathomechanisms in the neuronal ceroid lipofuscinoses. Biochim Biophys Acta Mol Basis Dis 2020;1866:165570. https://doi.org/10.1016/j.bbadis.2019.165570.

41. Nixon RA. The role of autophagy in neurodegenerative disease. Nat Med 2013;19:983–997. https://doi.org/10.1038/nm.3232.

42. Fraldi A, Klein AD, Medina DL, Settembre C. Brain disorders due to lysosomal dysfunction. Annu Rev Neurosci 2016;39:277–295. https://doi.org/10.1146/annurev-neuro-070815-014031.

43. Karageorgos LE, Isaac EL, Brooks DA, et al. Lysosomal biogenesis in lysosomal storage disorders. Exp Cell Res 1997;234:85–97. https://doi.org/10.1006/excr.1997.3581.

44. Saftig P, Puertollano R. How lysosomes sense, integrate, and cope with stress. Trends Biochem Sci 2021;46:97–112. https://doi.org/10.1016/j.tibs.2020.09.004.

45. Settembre C, Fraldi A, Medina DL, Ballabio A. Signals from the lysosome: a control centre for cellular clearance and energy metabolism. Nat Rev Mol Cell Biol 2013;14:283–296. https://doi.org/10.1038/nrm3565.